

1 Enhanced Mediterranean water cycle
2 explains increased humidity during MIS 3
3 in North Africa
4

5 Mike Rogerson¹

6 Yuri Dublyansky²

7 Dirk L. Hoffmann³

8 Marc Luetscher^{2,4}

9 Paul Töchterle²

10 Christoph Spötl²

11

12 1 School of Environmental Sciences, University of Hull, Cottingham Road, Hull, HU6 7RX, UK.

13 2 Institute of Geology, University of Innsbruck, Innrain 52, 6020 Innsbruck, Austria.

14 3 Department of Human Evolution, Max Planck Institute for Evolutionary Anthropology, Deutscher
15 Platz 6, 04103, Leipzig, Germany

16 4 Swiss Institute for Speleology and Karst Studies (ISSKA), Serre 68, CH-2300 La Chaux-de-Fonds

17

18 Abstract

19 *We report a new fluid inclusion dataset from Northeast Libyan speleothem SC-06-01, which is the*
20 *largest speleothem fluid inclusion dataset for North Africa to date. The stalagmite was sampled in*
21 *Susah cave, a low altitude coastal site, in Cyrenaica, on the northern slope of the Jebel Al-Akhdar.*
22 *Speleothem fluid inclusions from latest Marine Isotope Stage (MIS) 4 and throughout MIS 3 (~67 to*
23 *~30 ka BP) confirm the hypothesis that past humid periods in this region reflect westerly rainfall*
24 *advected through the Atlantic storm track. However, most of this moisture was sourced from the*
25 *Western Mediterranean, with little direct admixture of water evaporated from the Atlantic. Moreover,*
26 *we identify a second moisture source likely associated with enhanced convective rainfall within the*
27 *Eastern Mediterranean. The relative importance of the western and eastern moisture sources seems to*
28 *differ between the humid phases recorded in SC-06-01. During humid phases forced by precession,*
29 *fluid inclusions record compositions consistent with both sources, but the 52.5 – 50.5 ka interval*
30 *forced by obliquity reveals only a western source. This is a key result, showing that although the*
31 *amount of atmospheric moisture advections changes, the structure of the atmospheric circulation over*
32 *the Mediterranean does not fundamentally change during orbital cycles. Consequently, an arid belt*
33 *must have been retained between the Intertropical Convergence Zone and the mid-latitude winter*
34 *storm corridor during MIS 3 pluvials.*

35 Introduction

36 Atmospheric latent heat is a major component of global and regional climate energy budgets and
37 changes in its amount and distribution are key aspects of the climate system (Pascale et al., 2011).
38 Equally, in mid- and low-latitude regions, changes in the water cycle have more impact on landscapes
39 and ecosystems than changes in sensible heat (Black et al., 2010). Rainfall in semi-arid regions is thus
40 one of the key climate parameters that understanding future impact on human societies depends upon
41 (IPCC, 2014), making constraining of mid-latitude hydrology a globally significant research priority.
42 These regions, however, have a particularly sparse record of palaeoclimate due to typically poor
43 preservation of surface sedimentary archives (Swezey, 2001). North Africa is a region that fully

44 exhibits these limitations, and large areas present either no pre-Holocene record or else they present
45 highly discontinuous deposits indicating major reorganisation of the hydroclimate, which are
46 challenging to date (Armitage et al., 2007). North Africa also fully exhibits the progress
47 palaeoclimatologists have made in understanding continental hydrological change from its impact on
48 the marine system; our understanding of past North African hydroclimate is disproportionately drawn
49 from records from the Mediterranean Sea (Rohling et al., 2015) and the eastern Central Atlantic
50 (Goldsmith et al., 2017; deMenocal et al., 2000.; Adkins et al., 2006).

51 **Past changes in North African hydroclimate**

52 Marine-based evidence offers a coherent model in which changes in the spatial distribution of
53 insolation alter atmospheric circulation on orbital timescales (10^4 to 10^5 years) and force major
54 reorganisations of rainfall in semi-arid regions such as the Sahel and southern Saharan regions
55 (Rohling et al., 2015; Goldsmith et al., 2017). This result is at least partially confirmed in climate
56 modelling experiments (Bosmans et al., 2015; Tuenter et al., 2003) and provides a conceptual
57 framework in which fragmentary evidence of hydrological change on the adjacent continent can be
58 understood (Rowan et al., 2000). There is 1) strong geochemical evidence that runoff from the
59 African margin initiated the well-known “sapropel” thermohaline crises of the eastern Mediterranean
60 (Osborne et al., 2010; Osborne et al., 2008) and, 2) convincing evidence that the southern margin of
61 the Mediterranean was more variable than the northern in terms of the relative magnitude of
62 precipitation changes and the distribution of flora, fauna and hominid populations (Drake et al., 2011).
63 However, we emphasise the fact that this understanding is largely drawn from evidence from outside
64 continental North Africa, and that this limits our knowledge about the nature and impact of
65 hydrological changes in this region.

66 There is strong evidence for a more humid climate throughout the Sahara and Sahel regions during the
67 early Holocene (Gasse and Campo, 1994; Gasse, 2002; Fontes and Gasse, 1991; Prentice and Jolly,
68 2000; Jolly et al., 1998; Collins et al., 2017), and in older interglacial periods (Drake et al.,
69 2008; Armitage et al., 2007; Vaks et al., 2013). This evidence has been interpreted to indicate that
70 humid conditions extended from the modern Sahel (~15°N) to the Mediterranean coast (30-35°N).

71 However, this only partially agrees with model results, which do indicate orbitally forced migration of
72 the monsoon belt but not across such a large spatial scale as suggested by the empirical data. Model
73 experiments indicate that monsoonal rainfall occurring within the Intertropical Convergence Zone
74 (ITCZ) likely extended no further north than $\sim 23^{\circ}\text{N}$ (Harrison et al., 2015). This well-recognised lack
75 of agreement between rainfall fields in model experiments for the past and reconstructed
76 hydrographies from the distribution of lakes and vegetation (via pollen) (Peyron et al., 2006) remains
77 a major research problem. While some models also suggest that during times of high Northern
78 Hemisphere insolation, enhanced westerlies advected Atlantic moisture into the basin (Brayshaw et
79 al., 2009; Tuenter et al., 2003; Bosmans et al., 2015), high-resolution regional modelling indicates that
80 this primarily affected the northern Mediterranean margin (Brayshaw et al., 2009). This result is
81 consistent with evidence of enhanced runoff at these times from the southern margin of Europe
82 (Toucanne et al., 2015). On the African coast east of Algeria, the southern limit of enhanced
83 precipitation arising from increased westerly activity within model experiments essentially lies at the
84 coastline ($\sim 32^{\circ}\text{N}$), and does not appear to drive terrestrial hydrological changes. Overall, there is
85 therefore a striking mismatch between the apparent humidity of Africa between 23 and 32°N in the
86 empirical record (a zonally oriented belt ~ 1000 km in width) and the climate models. This region
87 encompasses southern Tunisia, in which multiple lines of evidence for distinct and widespread
88 periods of increased humidity provide a highly secure basis for enhanced rainfall during Northern
89 Hemisphere insolation maxima (Ballais, 1991; PETIT-MAIRE et al., 1991), the Fezzan basin, in
90 which compelling evidence for multiple lake highstands exists (Drake et al., 2011) and western Egypt,
91 where large tufa deposits attest to higher past groundwater tables (Smith et al., 2004).

92 An emerging picture of MIS 3 as a humid period within the Mediterranean basin is developing
93 (Langgut et al., 2018), and the current study focusses on this time period. However, MIS 3 is not well
94 expressed in the Sahara region. The Libyan interior is considered arid or even hyperarid throughout
95 the last glacial period (Cancellieri E. et al., 2016). Recent re-evaluation of palaeolake levels in
96 southwest Egypt indicates a groundwater-fed system active around 41 ka (Nicoll, 2018), which is
97 similar to dates for springline tufa systems at Kharga Oasis (Smith et al., 2007). We are not aware of

98 continental MIS 3 pollen records from the region, but marine pollen from Tunisia indicates more arid
99 conditions through the last glacial than during the Holocene (Brun, 1991). There is a triple peak in
100 runoff from the Nile recorded in the marine sediment record, with maxima at ~60, ~55 and ~35 ka,
101 indicating higher rainfall within the upper Nile catchment (Revel et al., 2010).

102 It is unlikely that significant further progress will be made in understanding the palaeoclimate of
103 North Africa without new empirical evidence of regional hydrological changes from which
104 atmospheric dynamics can be delineated.

105 The central North African speleothem record

106 Speleothem palaeoclimatology has high potential for North Africa, but is only recently becoming
107 established through key records developed for Morocco (Wassenburg et al., 2013; Ait Brahim et al.,
108 2017; Wassenburg et al., 2016). Until recently, the only speleothem record published from central
109 North Africa was a single continuous record from 20 to 6 ka BP from northern Tunisia (Grotte de la
110 Mine). This record shows a large deglacial transition in both $\delta^{13}\text{C}$ and $\delta^{18}\text{O}$ (Genty et al., 2006), with
111 oxygen isotopes indicating a 2-step change from a relatively isotopically heavy (-5‰) LGM (20-16 ka
112 BP), through an intermediate (-6 to -7‰) deglacial period (16-11.5 ka BP) to a relatively isotopically
113 light early Holocene. The $\delta^{13}\text{C}$ record indicates cool periods exhibiting higher carbon isotope values,
114 more clearly delineating the Bølling-Allerød / Younger Dryas oscillation than $\delta^{18}\text{O}$. This is assumed
115 to reflect higher soil respiration during warm periods (Genty et al., 2006). A major change in the
116 carbon isotopic composition occurred across the transition from the relatively arid glacial to the more
117 humid Early Holocene, and indicates a significant reorganisation of the regional hydroclimate.
118 However, it is difficult to interpret these data in isolation. A recently reported speleothem record (SC-
119 06-01) indicates that conditions in northern Libya during Marine Isotope Stage 3 (MIS 3) were more
120 humid than today, and shows isotopic evidence of a teleconnection between temperature in Greenland
121 and rainfall at the southern Mediterranean margin (Hoffmann et al., 2016). The oxygen isotope record
122 indicates that the water dripping into the cave during MIS 3 was isotopically too heavy for the
123 moisture to be sourced from within the monsoon system (Hoffmann et al., 2016). However, beyond
124 ruling out a southern source $\delta^{18}\text{O}_{\text{cc}}$ values alone are not sufficient to determine the origin of

125 atmospheric vapour. Three distinct humid phases within MIS3 are reported from this speleothem: 65-
126 61 ka, 52.5-50.5 ka and 37.5-33 ka. Phases I and III occur during times of low precession parameter,
127 when summer insolation on the northern hemisphere is relatively increased. Phase II represents the
128 first evidence for high obliquity being able to cause a pluvial period in the north African subtropics in
129 the same manner as precession (Hoffmann et al., 2016). In SC06-01, all three growth phases are
130 fractured into multiple short periods of growth, and show a marked temporal coherence with
131 Greenland Dansgaard-Oeschger interstadials (Hoffmann et al., 2016). Here, we report fluid inclusion
132 data from this speleothem and discuss how this helps resolve some of the issues discussed above.

133 **Fluid Inclusions**

134 Speleothem fluid inclusions are small volumes of water that were enclosed between or within calcite
135 crystals as they grew, ranging in size from less than 1 μm to hundreds of μm (Schwarcz et al., 1976).
136 This water represents quantities of ancient drip-water that can be interrogated directly to ascertain the
137 isotopic properties of the oxygen ($\delta^{18}\text{O}_{\text{fi}}$) and hydrogen ($\delta^2\text{H}_{\text{fi}}$) it comprises. This powerful approach
138 circumvents some of the uncertainty inherent in the interpretation of the stable isotopic values
139 preserved in the calcite comprising the speleothem itself ($\delta^{18}\text{O}_{\text{cc}}$, $\delta^{13}\text{C}_{\text{cc}}$). Fluid inclusion isotopes have
140 been used to demonstrate changes in air temperatures (Wainer et al., 2011; Meckler et al.,
141 2015; Arienzo et al., 2015) and in the origin of the moisture from which precipitation was sourced
142 (McGarry et al., 2004; Van Breukelen et al., 2008). Fluid inclusions from speleothems in Oman have
143 also been used to identify monsoon-sourced precipitation during interglacial phases (Fleitmann et al.,
144 2003), providing a rationale for similar investigation of fluid inclusion isotope behaviour in North
145 Africa.

146 In the case of fluid inclusions from northeastern Libyan speleothems, the boundary conditions for
147 atmospheric moisture supply are 1) the sea-surface temperature of the Atlantic and Mediterranean, 2)
148 the surface water $\delta^{18}\text{O}_{\text{sw}}$ of the same ocean regions, 3) land surface temperature of Africa and to a
149 lesser extent southern Europe, 4) insolation (especially with respect to ITCZ position) and 5) the zonal
150 pressure gradient across northern Africa.

151 **Modern rainfall system**

152 Modern rainfall in central North Africa is dominated by relatively wet winters, and summers with
153 little, if any, precipitation. Convective systems, cyclones, upper-level troughs and static instabilities
154 can all drive rainfall patterns in the Mediterranean basin and these modes are reviewed in (Dayan et
155 al., 2015). Convection essentially reflects the relatively high SST of the Mediterranean during the
156 winter, but rising air masses generally also need significant advection of moisture to drive significant
157 rainfall. Upper level troughs reflect large-scale circulation (e.g. Red Sea Trough) or reflect lee effects
158 downstream of mountains in the western Mediterranean, and promote rainfall in their regions of
159 formation. The dominant cyclogenetic centre is in the Gulf of Genoa, and secondary centres are placed
160 in south Italy, Crete and Cyprus. Cyclonic systems can also penetrate from the Atlantic, where the
161 high SST of the winter Mediterranean tends to sustain and amplify them, in close analogy to
162 convection forcing. The key static instability is the penetration of the tropical air mass into the
163 subtropical Mediterranean, forming a ‘Saharan Cloud Band’ at middle and upper atmospheric levels.
164 These originate from within the ITCZ. Libya is very sparsely instrumented, so we assume that
165 synoptic processes are similar to the Levant region. Here, most rainfall falls under winter, low
166 pressure conditions, and is convective (Peleg and Morin, 2012). The responsible low pressure systems
167 can relate to transient, shallow lows north of the area in which rainfall is occurring, or less frequently
168 more long-lasting Cyprus Lows or Red Sea Trough systems (Peleg and Morin, 2012).

169 **Material and Methods**

170 SC-06-01 is a 93-cm long stalagmite from Susah Cave (Fig. 1, 32°53.419’ N, 21°52.485’ E), which
171 lies on a steep slope ~200 m above sea level in the Al Akhdar massif in Cyrenaica, Libya (Fig. 1). The
172 region is semi-arid today, with mean annual temperature ~20°C and receiving less than 200 mm
173 precipitation per year, mostly in the winter (October to April). The Al Akhdar massif has thin soil
174 cover and a Mediterranean “maquis” vegetation. Susah Cave is hydrologically inactive today, and all
175 formations are covered with dust. The chronology of the speleothem and the general features of its
176 growth and $\delta^{18}\text{O}_{\text{cc}}$ record are published elsewhere (Hoffmann et al., 2016), and this study focuses on

177 fluid inclusion isotopes, their impact on the interpretation of $\delta^{18}\text{O}_{\text{cc}}$ and to a lesser extent on $\delta^{13}\text{C}_{\text{cc}}$ and
178 Sr isotopes.

179 Fluid inclusions were examined in doubly-polished thick section (100 μm) slides, using a Nikon
180 Eclipse E400 POL microscope. The isotope composition of fluid inclusion water was measured at the
181 University of Innsbruck using a Delta V Advantage IRMS coupled to a Thermal
182 Combustion/Elemental Analyser and a ConFlow II interface (Thermo Fisher) using the line, crusher
183 and cryo-focussing cell described in Dublyansky and Spötl (2009). Samples were cut with a diamond
184 band saw along visible petrographic boundaries in the speleothem, and therefore represent specific
185 growth increments. Samples were analysed at least in duplicate, with the standard sampling protocol
186 used on the Innsbruck instrument (Dublyansky and Spötl, 2009). To exclude the possibility of post-
187 depositional diagenetic alteration, petrographic thin sections were investigated using transmitted-light
188 microscopy. Results are detailed in Supplemental Information 1.

189 Optical emission spectroscopy (OES) was used to measure a variety of elemental concentrations,
190 including Sr, along the main growth axis of SC-06-01. The low spatial resolution of trace elemental
191 analyses (every 10 mm) does not allow to investigate time series of elemental variation but was useful
192 to assess Sr contents of the samples for Sr isotope measurements by thermal ionisation mass
193 spectrometry (TIMS). The samples for TIMS analyses were drilled using a hand held micro drill with
194 a tungsten carbide drill bit. Sample sizes range between 2 and 4 mg, thus we achieved a minimum Sr
195 load of 100 ng on the Re filaments for TIMS. Chemical sample preparation and subsequent TIMS
196 measurement were done following standard protocols (Charlier et al., 2006). No spike was added to
197 the samples prior to chemical purification. The Sr isotope measurements were done on a Triton TIMS
198 housed at the Bristol Isotope Group laboratory, University of Bristol.

199 Results

200 Fluid inclusions

201 Petrographic analysis of the thick sections indicates that the distribution of fluid inclusions is highly
202 variable, with macroscopically opaque “milky” calcite typical of rapidly growing intervals containing
203 sometimes very abundant inclusions and the discoloured, translucent calcite of the slowly growing
204 intervals being almost inclusion-free (Fig. 2). In most samples, two distinct populations of inclusions
205 were identified with numerous small intra-crystalline inclusions and larger, but less frequent, inter-
206 crystalline inclusions. Consequently, the volume of water analysed per sample was very variable (Fig.
207 3). Indeed, a significant proportion of individual fluid inclusion measurements had analyte volumes
208 too small ($<0.1 \mu\text{L}$) to have confidence in the isotope results. A small number of analyses failed due
209 to excessive water saturating the detector, and these have not been included in the datasets presented
210 here. The major impact of the highly variable availability of inclusions in the speleothem is a
211 significant bias in the analyses towards the most rapidly growing, and therefore probably humid, time
212 periods. Three rapidly-growing phases are reported in SC-06-01, named Phase I (62-67ka), Phase II
213 (53-50 ka) and Phase III (37-33 ka) (Hoffmann et al., 2016). Fluid inclusions for Phases I and III are
214 isotopically similar (with $\delta^{18}\text{O}_{\text{FI}}$ ranging from -7.5‰ to -3.8‰ and from -8.5‰ to -3.2‰
215 respectively and $\delta^2\text{H}_{\text{FI}}$ ranging from -26.7‰ to -18.6‰ and from -29.4‰ to -16.1‰ respectively).
216 However, compositions for Phase II are different, particularly with respect to deuterium ($\delta^{18}\text{O}_{\text{FI}}$
217 ranging from -8.9‰ to -4.5‰ and $\delta^2\text{H}_{\text{FI}}$ ranging from -38.3‰ to -25.1‰).

218 In most samples, achieving within-error replication ($\delta^2\text{H} \pm 1.5 \text{‰}$, $\delta^{18}\text{O}: \pm 0.5 \text{‰}$) of both $\delta^{18}\text{O}_{\text{fi}}$ and
219 $\delta^2\text{H}_{\text{fi}}$ was difficult. This must reflect more than one population of inclusions with different properties
220 being present within at least some samples, and each replicate analysis represents some proportion of
221 mixing between these populations. This suggests significant short-term variability in the composition
222 of the water stored in the presumably rather small soil/epikarst zone overlying the cave.

223 Consequently, any given time interval risks being under-sampled with regard to variability at that
224 time. Although there is some visual correspondence between the $\delta^{18}\text{O}_{\text{fi}}$, $\delta^2\text{H}_{\text{fi}}$ and $\delta^{18}\text{O}_{\text{cc}}$ data series

225 (Fig. 4), it seems that the fluid inclusion time series risks aliasing changes seen in the calcite isotope
226 time series. Consequently, the usefulness of interpretation that can be drawn from the episodic SC-01-
227 06 fluid inclusion dataset when arranged as a time series is limited and we therefore largely focus our
228 discussion to the properties of the population of waters as a full dataset. This approach minimises the
229 impact the different populations can have on interpretation.

230 Figure 5 shows the SC-06-01 fluid inclusion dataset alongside Global Network of Isotopes in
231 Precipitation (GNIP) datasets from Tunis World Meteorological Office (WMO station 6071500), Sfax
232 (6075000) and Bet Dagan (4017900) (locations in Fig. 1) and other published precipitation datasets.
233 The Tunisian datasets fit within a trend typical of the Global Meteoric Water Line (GMWL) ($\delta^2\text{H} =$
234 $8\delta^{18}\text{O} + 10$). However, all this data lies along a single moisture evolution trend, and the Tunis and
235 Sfax populations overlap. The data from Bet Dagan exhibits a trend which is extremely close to being
236 parallel to the global trend dominating in Tunisia, but translated by +10 ‰ in $\delta^2\text{H}$, reflecting greater
237 deuterium excess. This is typical of the Mediterranean Meteoric Water Line (MMWL) (Ayalon et al.,
238 1998; Gat et al., 2003), and reflects internal recycling of water with consequent deuterium enrichment
239 in the eastern Mediterranean and its bordering continental areas.

240 The values of $\delta^2\text{H}_{\text{fi}}$ and $\delta^{18}\text{O}_{\text{fi}}$ fit within the range of values for modern precipitation, giving
241 confidence that these measurements do reflect past precipitation composition despite the influence of
242 multiple inclusion populations. The lack of apparent scatter towards positive $\delta^{18}\text{O}$ values both in the
243 precipitation and fluid inclusion datasets further indicates that the data represent little-altered
244 precipitation values, and that surface re-evaporation was minor at least during humid phases.

245 However, the range of fluid inclusion values is inconsistent with either an exclusively Tunis-type or
246 an exclusively Bet Dagan-type moisture source for precipitation in Cyrenaica during MIS 3. Even
247 when all but the subset of fluid inclusion analyses who replicates are similar are excluded (Fig. 6), the
248 population is split between the Tunisian and Israeli precipitation end-members.

249 **Strontium isotopes**

250 The $^{87}\text{Sr}/^{86}\text{Sr}$ signal in the SC-06-01 record is rather invariable (Fig. 7), with all analyses indicating
251 values within analytical error. Mean values vary between 0.708275 and 0.708524 and although there
252 is an apparent trend from maxima at 34 and 64 ka BP with a minimum at 52 ka BP, which mimics the
253 precession history, this is too weak to be significant relative to the error.

254 **Calcite carbon isotopes**

255 Both $\delta^{13}\text{C}_{\text{cc}}$ and $\delta^{18}\text{O}_{\text{cc}}$ show similar trends throughout the record (Fig. 8), indicating that depleted
256 oxygen isotopes coincide with depleted carbon isotope values. This does not appear to arise from
257 fractionation on the speleothem surface (Hoffmann et al., 2016), and so represents changes in soil
258 bioproductivity acting in concert with changes in precipitation.

259 **Discussion**

260 **Moisture advection during Libyan humid phases**

261 The range of values of both individual and replicated fluid inclusion measurements can only be
262 reconciled with multiple moisture sources. Most of the fluid inclusion data cluster between the
263 weighted mean value for precipitation collected at Sfax with a mixed source from the Atlantic and
264 western Mediterranean, (“Sfax Mixed” $\delta^{18}\text{O}_{\text{ppt}} = -4.93 \text{ ‰}$, $\delta^2\text{H}_{\text{ppt}} = -26 \text{ ‰}$; Fig. 9) and High
265 Precipitation events at Bet Dagan ($\delta^{18}\text{O}_{\text{ppt}} = -6.33 \text{ ‰}$, $\delta^2\text{H}_{\text{ppt}} = -21.46 \text{ ‰}$; Fig. 9). However, the fluid
266 inclusion data cluster also extends to the end member reflecting pure western Mediterranean sources
267 at Sfax ($\delta^{18}\text{O}_{\text{ppt}} = -3.99 \text{ ‰}$, $\delta^2\text{H}_{\text{ppt}} = -20.3 \text{ ‰}$; Fig. 9), indicating a third end member composition with
268 higher $\delta^{18}\text{O}_{\text{ppt}}$. The weighted mean value for Atlantic-sourced precipitation events in Sfax ($\delta^{18}\text{O}_{\text{ppt}} = -$
269 6.7 ‰ , $\delta^2\text{H}_{\text{ppt}} = -37.7 \text{ ‰}$) is distant from any observed fluid inclusion value (Fig. 9). A simple 3-end-
270 member unmixing of fluid inclusion isotope values using the quantitative approach of (Rogerson et
271 al., 2011) indicates that Atlantic-sourced water supplied no more than 15 % of the mass for any given
272 fluid inclusion analysis. However, the coherence of fluid inclusion isotope ratios with the weighted
273 mean of “mixed” Atlantic and Mediterranean precipitation at Sfax suggests that this small Atlantic

274 influence is nevertheless persistent, and this must reflect synoptic westerly storms (Celle-Jeanton et
275 al., 2001).

276 The simplest interpretation of the Susah Cave fluid inclusion data is therefore that they reflect a
277 dynamic balance of moisture sources contributing to rainfall in Cyrenaica which resembles modern
278 precipitation in Tunisia and Israel in roughly equal proportions. An alternative way to explain the
279 trend of some points towards enriched $\delta^{18}\text{O}$ values on the GMWL would be the temperature-
280 dependent fractionation that would be caused by a shift to summertime precipitation. We do not
281 favour this explanation, as it requires a more fundamental reorganisation of regional atmospheric
282 circulation than our suggestion that the winter storms observed today penetrated further east in the
283 past.

284 Although the isotopic composition of Mediterranean water will have been more enriched during MIS
285 3 due to ice-volume effects and increased Mediterranean water residence time (Rohling and Bryden,
286 1994), the similar mean values of the SC-06-01 fluid inclusion waters compared to modern
287 precipitation indicates the meteoric waterline at this time was not displaced to more enriched isotope
288 values. This could reflect balancing of source water effects by changes in kinetic fractionation during
289 evaporation (Goldsmith et al., 2017), which is controlled by normalised relative humidity. This would
290 imply that the Mediterranean air masses were less saturated with moisture than today during MIS 3,
291 which is consistent with the high deuterium excess $\delta^2\text{H}_{\text{excess}}$ values found in some fluid inclusion
292 samples (Fig. 10), but is difficult to reconcile with the increased precipitation recorded in SC-06-01.
293 In addition, changes in cloud height and cloud formation processes could possibly alter the isotopic
294 fractionation in the atmosphere. Alternatively, the source water effect may be countered by increased
295 runoff from the margins of the Mediterranean supplying isotopically depleted water to evaporating
296 surface water. Isotopic “residuals” consistent with this argument are identified throughout MIS 3 in
297 the eastern Mediterranean marine core LC21 (Grant et al., 2016), and this is also consistent with
298 higher rainfall in Cyrenaica. We therefore favour the latter explanation.

299 Although we find that our results likely reflect patterns of atmospheric transport in MIS 3 comparable
300 to today, it is possible that some moisture was drawn from re-evaporation of monsoon rain falling

301 further south, with no modern analogue in the region (Aggarwal et al., 2016). This water would likely
302 be extremely isotopically light, reflecting both monsoon-type compositions and further fractionation
303 during secondary evaporation. Moreover, a shift to more southerly-sourced regions is inconsistent
304 with Sr-isotope data from Susah Cave. Sr-isotopes are known to be sensitive to changes in transport of
305 Saharan dust (Frumkin and Stein, 2004), but even considering the most slowly-growing and most
306 rapidly-growing parts of SC-06-01, no significant difference in $^{87}\text{Sr}/^{86}\text{Sr}$ has been identified. Although
307 at times of extreme rainfall in the region, Saharan/Sahellian dust production is suppressed, this is not
308 true during MIS 3 (Collins et al., 2013). It seems that despite changes in the intensity of moisture
309 transport during the period 65-30 ka BP, there is no large-scale change in atmospheric dust transport
310 direction. This further supports our conclusion from the fluid inclusions that the Eastern
311 Mediterranean rainfall operating during precession parameter minima reflects enhanced internal
312 convection rather than transport of moisture from the east or south with an atmospheric circulation
313 pattern that prevails today.

314 Different sources at different times?

315 Phase II fluid inclusions are exceptional, because none show compositions consistent with a Bet
316 Dagan source. This is most clearly reflected in the $\delta^2\text{H}_{\text{excess}}$ values (Fig. 10), which show consistently
317 low values across Phase II comparing well to the Western water end-member (~10 ‰) and not the
318 Eastern water end-member (~30 ‰). The lack of Eastern water during Phase II seems to reflect a
319 fundamental difference between this period and Phases I and III, as during this time all precipitation
320 was drawn from synoptic westerly storms in the winter. Consequently, it would seem that during the
321 obliquity-forced period of humidity, the Israeli-mode precipitation did not occur in the manner that it
322 did during both precession-forced periods of humidity. This difference in the origin of the moisture
323 feeding rainfall may explain the difference in average $\delta^{18}\text{O}_{\text{cc}}$ during these different phases (Hoffmann
324 et al., 2016), and why some periods in Susah Cave show strong correlation with North Atlantic
325 temperature whereas others do not (Hoffmann et al., 2016).

326 **Palaeoclimatological significance**

327 Most of the precipitation supplied to Cyrenaica during MIS 3 was sourced from within the
328 Mediterranean basin, which exhibited a similar meteoric water cycle to that observed today, albeit
329 with more freshwater influence. This is a critical observation, as the precipitation feeding runoff must
330 be externally sourced if it is to materially change Mediterranean functioning, as is observed during
331 sapropel events (Rohling et al., 2015). The internally-cycled water we report from Susah Cave cannot
332 alter the basin-scale hydrological balance, and therefore is a minor influence on deep convection in
333 the Mediterranean Sea (Bethoux and Gentili, 1999): put simply, this means evidence of increased
334 rainfall in the coastal Mediterranean does not provide evidence for decreased net evaporation in the
335 marine system. This observation is critical, as it decouples the processes of precipitation on the
336 Mediterranean margins with sapropel formation, and consequent changes in momentum transfer to the
337 North Atlantic (Rogerson et al., 2012).

338 Despite the low level of Atlantic moisture contributing to rainfall in Libya in MIS 3, the Western-
339 sourced moisture is transported ~1500 km eastwards to reach Cyrenaica, which must reflect the mid-
340 latitude storm track (Brayshaw et al., 2009). Consequently, although it does not seem that Atlantic
341 moisture is important to the climatology of Cyrenaica, the momentum derived from Atlantic winter
342 storms predicted by regional climate modelling (Brayshaw et al., 2009) and observed on the northern
343 Mediterranean margin (Toucanne et al., 2015) remains pivotal to supplying moisture to North Africa.
344 Consequently, the North Atlantic heat budget provides an important control on northern African
345 rainfall in the past. In contrast, this control cannot explain changes in the Eastern-sourced rainfall
346 revealed by our analysis. Eastern-sourced rainfall may occasionally relate to wintertime storms, as
347 today (Gat et al., 2003), but essentially reflects convective rainfall with relatively small advection
348 distances. It is likely this arises due to greater atmospheric convergence due to northward
349 displacement of the annual average position of the ITCZ (Tuenter et al., 2003).

350 Palaeoclimatologically, our analysis reveals that 1) during northern hemisphere insolation peaks
351 reflecting precession, coastal Libya experiences greater westerly advection of water due to an increase
352 in Atlantic heat and greater convective rainfall due to migration of the ITCZ, whereas 2) insolation

353 peaks reflecting obliquity show increased Atlantic heat and westerlies, but no comparable change in
354 the ITCZ position.

355 *Implications for Susah Cave $\delta^{18}O_{cc}$*

356 Aside from those data with high deuterium excess, which reflect influence from the Eastern
357 Mediterranean source, much of the variance in the fluid inclusion dataset is captured by a two end-
358 member mixing system resembling modern rainfall in Tunisia. One end-member is the Western
359 Mediterranean source of Celle-Jeanton et al. (2001), but the other is isotopically too heavy to be
360 identified with the Atlantic source. Rather, it resembles the “Sfax Mixed” population defined by
361 Celle-Jeanton et al. (2001), reflecting a mixed source of moisture from both the Western
362 Mediterranean and Atlantic. Consequently, although quantitatively minor amounts of Atlantic water
363 reached the site, changes in the moisture advection driven by westerly winds had a strong influence on
364 $\delta^{18}O_{dripwater}$ trends in time. At Sfax today, this influence causes a prominent bimodal behaviour with
365 two rainfall maxima with different $\delta^{18}O_{ppt}$, which eliminates a simple and quantitative rainfall amount
366 control on precipitation as observed at Tunis (WMO code 6071500,
367 <https://nucleus.iaea.org/wiser/gnip.php>). Furthermore, addition of heavy rain events derived from the
368 Eastern Mediterranean aliases the tendency towards depleted $\delta^{18}O_{dripwater}$, as this water is also more
369 depleted than modern Western Mediterranean precipitation. In the Bet Dagan data, there is also a
370 tendency to lower $\delta^{18}O_{ppt}$ with higher precipitation amount, but the relationship between rainfall
371 amount and rainfall isotope composition is not identical to Tunis. Ultimately, it seems likely that
372 rainfall amount changes at Susah Cave do cause depleted (enriched) $\delta^{18}O_{cc}$ values to be associated
373 with high (low) rainfall, but this is too complicated by independent changes in westerly moisture
374 advection and in convergence. Qualitatively, all these parameters are expected symptoms of North
375 African humid phases and so these trends remain a valuable expression of climatic variability.
376 Quantitatively, more information is required to translate the trends into fully-functional
377 palaeoclimatologies, and this analysis pivots on whether $\delta^{18}O_{cc}$ trends reflect changes in water deficit /
378 surplus in Cyrenaica.

379 Although it is likely the oxygen isotope fractionation during calcite precipitation occurred close to
380 isotope equilibrium (Hoffmann et al., 2016), there is a good degree of correspondence between
381 positive and negative phases in $\delta^{18}\text{O}_{\text{cc}}$ and $\delta^{13}\text{C}_{\text{cc}}$, indicating a shared control. Indeed, $\delta^{13}\text{C}_{\text{cc}}$ has a
382 markedly higher amplitude variability than $\delta^{18}\text{O}_{\text{cc}}$. More isotopically depleted carbon may represent
383 increased incorporation of respired soil carbon, increased dominance of C3 over C4 plants, and/or
384 decreased degassing of aquifer water (Baker et al., 1997). Today, the Susah Cave location on Jebel
385 Malh has very thin soil cover, colonised by shrubby maquis vegetation. Soil respiration and
386 colonisation by C3 plants is limited by the strong water deficit of the region, and aquifer water
387 outgassing is enhanced by long residence times due to low water infiltration. Increased water
388 availability will progressively deplete the $\delta^{13}\text{C}$ of dripwater by all three mechanisms described above.
389 Consequently, all three of these processes promote correlation between $\delta^{13}\text{C}_{\text{cc}}$ and precipitation
390 amount. Within the $\delta^{18}\text{O}_{\text{cc}}$ data series, peak growth rates occur both during relatively enriched and
391 relatively depleted isotope stages. This is not the case for $\delta^{13}\text{C}_{\text{cc}}$, which more consistently shows
392 depleted values during times of rapid growth (SC-06-01 growth phases shown in Fig. 11). We
393 therefore consider it likely that $\delta^{13}\text{C}_{\text{cc}}$ indeed more accurately records rainfall amount than $\delta^{18}\text{O}_{\text{cc}}$ does.

394 Conclusions and Implications

395 A key feature of this combined dataset is the long-term sinusoidal trend in both the $\delta^{18}\text{O}_{\text{cc}}$ and $\delta^2\text{H}_{\text{fi}}$,
396 reflecting the differing rainfall regimes dominant between Humid Phases I and III compared to Phase
397 II. This is not developed in $\delta^{13}\text{C}_{\text{cc}}$, implying that the process forcing the long-term cycle in moisture
398 source is not impacting on carbon dynamics in the soil and epikarst. We therefore conclude that there
399 is a mixed amount and source control on $\delta^{18}\text{O}$ and $\delta^2\text{H}$ in the SC-01-06 record, whereas $\delta^{13}\text{C}$ is
400 dominantly controlled by water availability.

401 The fluid inclusions from SC-06-01 show that rainfall compositions in the southeast Mediterranean
402 region during MIS 3 were comparable to modern rainfall compositions recorded in regional GNIP
403 datasets. However, the diversity of compositions is impossible to explain with a single rainfall source,
404 rather indicating that moisture derived from the Atlantic, the Western Mediterranean and the Eastern

405 Mediterranean basins have all contributed to MIS 3 precipitation in Libya. This requires both
406 enhanced westerly advection of moisture to this region, reflecting the Atlantic storm track, and
407 enhanced convective rainfall within the Eastern Mediterranean basin. There is some indication that
408 these two mechanisms differ in terms of their response to orbital forcing, with precession parameter
409 minima enhancing westerly advection and internal convection, whereas obliquity minima enhance
410 westerly advection without significantly altering internal convection.

411 Crucially, this picture is most consistent with atmospheric circulation over the Mediterranean
412 remaining essentially unchanged during precession cycles. This is consistent with regional climate
413 model experiments showing major enhancement of winter westerly storm activity, but it is not
414 consistent with the extreme migration of the ITCZ, where the monsoon belt approaches the North
415 African coast. The strong implication is that a significant arid belt is retained between the
416 Mediterranean and the ITCZ, even when northernmost Africa is experiencing significantly enhanced
417 rainfall.

418 It is likely that rainfall amount played a role in controlling the isotopic composition of the calcite in
419 this speleothem ($\delta^{18}\text{O}_{\text{cc}}$). However, the more depleted values reflecting higher rainfall are also
420 consistent with different mixing between the end members identified by the fluid inclusion analysis.
421 The structure of the $\delta^{13}\text{C}_{\text{cc}}$ record provides an independent means of assessing changes in water
422 surplus / deficit, as more depleted values will reflect lower aquifer residence times, enhanced soil
423 respiration and changes in vegetation structure, all of which are limited by water availability in this
424 semi-arid environment. Combined analysis of the proxies provides a powerful new demonstration that
425 the northeast Libyan climate was more humid during millennial-scale warm periods in the North
426 Atlantic realm, but quantification will be dependent on generating unambiguous independent evidence
427 for water availability in the soil and epikarst.

428 Acknowledgements

429 We thank the Royal Geographical Society for the pump-priming investment that began this work
430 (Thesiger-Oman International Fellowship 2009), the Natural Environment Research Council for

431 providing the funds that made the analytical work on this project possible (NE/J014133/1) and The
432 Leverhulme Trust for funding activities within the associated International Network (IN-2012-113).
433 We also thank two anonymous reviewers for considerably improving the quality and accessibility of
434 this paper.

435 References

- 436 Arienzo, M.M. et al. 2015. Bahamian speleothem reveals temperature decrease associated with
437 Heinrich stadials. *EPSL* 430, 377-386.
- 438 Adkins, J., Demenocal, P., and Eshel, G.: The "African humid period" and the record of marine
439 upwelling from excess ^{230}Th in Ocean Drilling Program Hole 658C, *Paleoceanography and*
440 *Paleoclimatology*, 21, 2006.
- 441 Aggarwal, P. K., Romatschke, U., Araguas-Araguas, L., Belachew, D., Longstaffe, F. J., Berg, P.,
442 Schumacher, C., and Funk, A.: Proportions of convective and stratiform precipitation revealed in
443 water isotope ratios, *Nat. Geosci.*, 9, 624, 2016.
- 444 Ait Brahim, Y., Cheng, H., Sifeddine, A., Wassenburg, J. A., Cruz, F. W., Khodri, M., Sha, L., Pérez-
445 Zanón, N., Beraaouz, E. H., Apaéstegui, J., Guyot, J.-L., Jochum, K. P., and Bouchaou, L.: Speleothem
446 records decadal to multidecadal hydroclimate variations in southwestern Morocco during the last
447 millennium, *Earth and Planetary Science Letters*, 476, 1-10,
448 <https://doi.org/10.1016/j.epsl.2017.07.045>, 2017.
- 449 Arienzo, M. M., Swart, P. K., Pourmand, A., Broad, K., Clement, A. C., Murphy, L. N., Vonhof, H. B.,
450 and Kakuk, B.: Bahamian speleothem reveals temperature decrease associated with Heinrich
451 stadials, *Earth and Planetary Science Letters*, 430, 377-386, 2015.
- 452 Armitage, S. J., Drake, N. A., Stokes, S., El-Hawat, A., Salem, M., White, K., Turner, P., and McLaren, S.
453 J.: Multiple phases of north African humidity recorded in lacustrine sediments from the fazzan basin,
454 Libyan sahara, *Quaternary Geochronology*, 2, 181-186, 2007.
- 455 Ayalon, A., Bar-Matthews, M., and Sass, E.: Rainfall-recharge relationships within a karstic terrain in
456 the Eastern Mediterranean semi-arid region, Israel: $\delta^{18}\text{O}$ and δD characteristics, *Journal of*
457 *Hydrology*, 207, 18-31, 10.1016/S0022-1694(98)00119-X, 1998.
- 458 Baker, A., Ito, E., Smart, P. L., and McEwan, R. F.: Elevated and variable values of ^{13}C in speleothems
459 in a British cave system, *Chemical Geology*, 136, 263-270, 1997.
- 460 Ballais, J.-L.: Evolution holocène de la Tunisie saharienne et présaharienne, *Méditerranée*, 74, 31-38,
461 1991.
- 462 Bethoux, J. P., and Gentili, B.: Functioning of the Mediterranean Sea: past and present changes
463 related to freshwater input and climate changes, *Journal of Marine Systems*, 20, 33-47, 1999.
- 464 Black, E., Brayshaw, D. J., and Rambeau, C. M. C.: Past, present and future precipitation in the Middle
465 East: Insights from models and observations, *Philosophical Transactions of the Royal Society A:*
466 *Mathematical, Physical and Engineering Sciences*, 368, 5173-5184, 10.1098/rsta.2010.0199, 2010.
- 467 Bosmans, J. H. C., Drijfhout, S. S., Tuenter, E., Hilgen, F. J., Lourens, L. J., and Rohling, E. J.: Precession
468 and obliquity forcing of the freshwater budget over the Mediterranean, *Quaternary Science*
469 *Reviews*, 123, 16-30, 10.1016/j.quascirev.2015.06.008, 2015.
- 470 Brayshaw, D. J., Woollings, T., and Vellinga, M.: Tropical and Extratropical Responses of the North
471 Atlantic Atmospheric Circulation to a Sustained Weakening of the MOC, *Journal of Climate*, 22, 3146-
472 3155, 10.1175/2008jcli2594.1, 2009.
- 473 Brun, A.: Reflections on the pluvial and arid periods of the Upper Pleistocene and of the Holocene in
474 Tunisia, *Palaeoecology of Africa and the surrounding islands*. Vol. 22. Proc. symposium on African
475 palynology, Rabat, 1989, 157-170, 1991.

476 Cancellieri E., Cremaschi M., Zerboni A., and S., d. L.: Climate, Environment, and Population
477 Dynamics in Pleistocene Sahara, in: Africa from MIS 6-2. Vertebrate Paleobiology and
478 Paleoanthropology. , edited by: Jones S., and B., S., Springer, Dordrecht, 2016.

479 Celle-Jeanton, H., Zouari, K., Travi, Y., and Daoud, A.: Caractérisation isotopique des pluies en
480 Tunisie. Essai de typologie dans la région de Sfax, Sciences de la Terre et des planètes, 333, 625-631,
481 2001.

482 Charlier, B., Ginibre, C., Morgan, D., Nowell, G., Pearson, D., Davidson, J., and Ottley, C.: Methods for
483 the microsampling and high-precision analysis of strontium and rubidium isotopes at single crystal
484 scale for petrological and geochronological applications, Chemical Geology, 232, 114-133, 2006.

485 Collins, J. A., Govin, A., Mulitza, S., Heslop, D., Zabel, M., Hartmann, J., Röhl, U., and Wefer, G.:
486 Abrupt shifts of the Sahara–Sahel boundary during Heinrich stadials, Climate of the Past, 9, 1181-
487 1191, 2013.

488 Collins, J. A., Prange, M., Caley, T., Gimeno, L., Beckmann, B., Mulitza, S., Skonieczny, C., Roche, D.,
489 and Schefuß, E.: Rapid termination of the African humid period triggered by northern high-latitude
490 cooling, Nature Communications, 8, 1372, 2017.

491 Dayan, U., Nissen, K., and Ulbrich, U.: Review Article: Atmospheric conditions inducing extreme
492 precipitation over the eastern and western Mediterranean, Nat. Hazards Earth Syst. Sci., 15, 2525-
493 2544, 10.5194/nhess-15-2525-2015, 2015.

494 deMenocal, P., Ortiz, J., Guilderson, T., Adkins, J., Sarnthein, M., Baker, L., and Yarusinsky, M.: Abrupt
495 onset and termination of the African Humid Period: rapid climate responses to gradual insolation
496 forcing. , Quaternary Science Reviews, 19, 347- 361, 2000.

497 Drake, N. A., El-Hawat, A. S., Turner, P., Armitage, S. J., Salem, M. J., White, K. H., and McLaren, S.:
498 Palaeohydrology of the Fazzan Basin and surrounding regions: The last 7 million years,
499 Palaeogeography Palaeoclimatology Palaeoecology, 263, 131-145, 10.1016/j.palaeo.2008.02.005,
500 2008.

501 Drake, N. A., Blench, R. M., Armitage, S. J., Bristow, C. S., and White, K. H.: Ancient watercourses and
502 biogeography of the Sahara explain the peopling of the desert, Proc. Natl. Acad. Sci. U. S. A., 108,
503 458-462, 10.1073/pnas.1012231108, 2011.

504 Dublyansky, Y. V., and Spötl, C.: Hydrogen and oxygen isotopes of water from inclusions in minerals:
505 Design of a new crushing system and on-line continuous-flow isotope ratio mass spectrometric
506 analysis, Rapid Communications in Mass Spectrometry, 23, 2605-2613, 10.1002/rcm.4155, 2009.

507 Fleitmann, D., Burns, S. J., Neff, U., Mangini, A., and Matter, A.: Changing moisture sources over the
508 last 330,000 years in Northern Oman from fluid-inclusion evidence in speleothems, Quaternary
509 Research, 60, 223-232, [http://dx.doi.org/10.1016/S0033-5894\(03\)00086-3](http://dx.doi.org/10.1016/S0033-5894(03)00086-3), 2003.

510 Fontes, J. C., and Gasse, F.: PALHYDAF (Palaeohydrology in Africa) program: objectives, methods,
511 major results, Palaeogeography, Palaeoclimatology, Palaeoecology, 84, 191-215, 10.1016/0031-
512 0182(91)90044-R, 1991.

513 Frumkin, A., and Stein, M.: The Sahara-East Mediterranean dust and climate connection revealed by
514 strontium and uranium isotopes in a Jerusalem speleothem, Earth and Planetary Science Letters,
515 217, 451-464, 10.1016/S0012-821X(03)00589-2, 2004.

516 Gasse, F., and Campo, E. v.: Abrupt post-glacial climate events in west Asia and north Africa
517 monsoon domains, Earth and Planetary Science Letters, 126, 435-456, 1994.

518 Gasse, F.: Diatom-inferred salinity and carbonate oxygen isotopes in Holocene waterbodies of the
519 western Sahara and Sahel (Africa), Quaternary Science Reviews, 21, 737-767, 2002.

520 Gat, J. R., Klein, B., Kushnir, Y., Roether, W., Wernli, H., Yam, R., and Shemesh, A.: Isotope
521 composition of air moisture over the Mediterranean Sea: An index of the air-sea interaction pattern,
522 Tellus, Series B: Chemical and Physical Meteorology, 55, 953-965, 10.1034/j.1600-
523 0889.2003.00081.x, 2003.

524 Genty, D., Blamart, D., Ghaleb, B., Plagnes, V., Causse, C., Bakalowicz, M., Zouari, K., Chkir, N.,
525 Hellstrom, J., Wainer, K., and Bourges, F.: Timing and dynamics of the last deglaciation from

526 European and North African $\delta^{13}\text{C}$ stalagmite profiles-comparison with Chinese and South
527 Hemisphere stalagmites, *Quaternary Science Reviews*, 25, 2118-2142, 2006.

528 Goldsmith, Y., Polissar, P. J., Ayalon, A., Bar-Matthews, M., deMenocal, P. B., and Broecker, W. S.:
529 The modern and Last Glacial Maximum hydrological cycles of the Eastern Mediterranean and the
530 Levant from a water isotope perspective, *Earth and Planetary Science Letters*, 457, 302-312,
531 <http://dx.doi.org/10.1016/j.epsl.2016.10.017>, 2017.

532 Grant, K. M., Grimm, R., Mikolajewicz, U., Marino, G., Ziegler, M., and Rohling, E. J.: The timing of
533 Mediterranean sapropel deposition relative to insolation, sea-level and African monsoon changes,
534 *Quaternary Science Reviews*, 140, 125-141, <http://dx.doi.org/10.1016/j.quascirev.2016.03.026>,
535 2016.

536 Harrison, S., Bartlein, P., Izumi, K., Li, G., Annan, J., Hargreaves, J., Braconnot, P., and Kageyama, M.:
537 Evaluation of CMIP5 palaeo-simulations to improve climate projections, *Nature Climate Change*, 5,
538 735-743, 2015.

539 Hoffmann, D. L., Rogerson, M., Spötl, C., Luetscher, M., Vance, D., Osborne, A. H., Fello, N. M., and
540 Moseley, G. E.: Timing and causes of North African wet phases during MIS 3 and implications for
541 Modern Human migration, *Nature Scientific Reports*, 6, 36367, 2016.

542 IPCC: Climate Change 2014: Impacts, Adaptation, and Vulnerability. Part B: Regional Aspects.
543 Contribution of Working Group II to the Fifth Assessment Report of the Intergovernmental Panel on
544 Climate Change, United Kingdom and New York, 688, 2014.

545 Jolly, D., Prentice, I. C., Bonnefille, R., Ballouche, A., Bengo, M., Brenac, P., Buchet, G., Burney, D.,
546 Cazet, J. P., Cheddadi, R., Ederh, T., Elenga, H., Elmoutaki, S., Guiot, J., Laarif, F., Lamb, H., Lezine, A.
547 M., Maley, J., Mbenza, M., Peyron, O., Reille, M., Reynaud-Farrera, I., Riollet, G., Ritchie, J. C., Roche,
548 E., Scott, L., Ssemmanda, I., Straka, H., Umer, M., Van Campo, E., Vilimumbalo, S., Vincens, A., and
549 Waller, M.: Biome reconstruction from pollen and plant macrofossil data for Africa and the Arabian
550 peninsula at 0 and 6000 years, *Journal of Biogeography*, 25, 1007-1027, 1998.

551 Langgut, D., Almogi-Labin, A., Bar-Matthews, M., Pickarski, N., and Weinstein-Evron, M.: Evidence
552 for a humid interval at ~56–44 ka in the Levant and its potential link to modern humans dispersal
553 out of Africa, *Journal of Human Evolution*, 124, 75-90, [10.1016/j.jhevol.2018.08.002](http://dx.doi.org/10.1016/j.jhevol.2018.08.002), 2018.

554 McGarry, S., Bar-Matthews, M., Matthews, A., Vaks, A., Schilman, B., and Ayalon, A.: Constraints on
555 hydrological and paleotemperature variations in the Eastern Mediterranean region in the last 140 ka
556 given by the δD values of speleothem fluid inclusions, *Quaternary Science Reviews*, 23, 919-934,
557 <http://dx.doi.org/10.1016/j.quascirev.2003.06.020>, 2004.

558 Meckler, A. N., Affolter, S., Dublyansky, Y. V., Krüger, Y., Vogel, N., Bernasconi, S. M., Frenz, M.,
559 Kipfer, R., Leuenberger, M., Spötl, C., Carolin, S., Cobb, K. M., Moerman, J., Adkins, J. F., and
560 Fleitmann, D.: Glacial–interglacial temperature change in the tropical West Pacific: A comparison of
561 stalagmite-based paleo-thermometers, *Quaternary Science Reviews*, 127, 90-116,
562 <http://dx.doi.org/10.1016/j.quascirev.2015.06.015>, 2015.

563 Nicoll, K.: A revised chronology for Pleistocene paleolakes and Middle Stone Age – Middle Paleolithic
564 cultural activity at Bîr Tîrfawi – Bîr Sahara in the Egyptian Sahara, *Quaternary International*, 463, 18-
565 28, <https://doi.org/10.1016/j.quaint.2016.08.037>, 2018.

566 Osborne, A., Vance, D., Rohling, E., Barton, N., Rogerson, M., and Fello, N.: A humid corridor across
567 the Sahara for the migration of early modern humans out of Africa 120,000 years ago, *Proc. Natl.*
568 *Acad. Sci. U. S. A.*, doi_10.1073_pnas.0804472105, 2008.

569 Osborne, A. H., Marino, G., Vance, D., and Rohling, E. J.: Eastern Mediterranean surface water Nd
570 during Eemian sapropel S5: monitoring northerly (mid-latitude) versus southerly (sub-tropical)
571 freshwater contributions, *Quaternary Science Reviews*, 29, 2473-2483,
572 <http://dx.doi.org/10.1016/j.quascirev.2010.05.015>, 2010.

573 Pascale, S., Gregory, J. M., Ambaum, M., and Tailleux, R.: Climate entropy budget of the HadCM3
574 atmosphere-ocean general circulation model and of FAMOUS, its low-resolution version, *Climate*
575 *Dynamics*, 36, 1189-1206, [10.1007/s00382-009-0718-1](https://doi.org/10.1007/s00382-009-0718-1), 2011.

576 Peleg, N., and Morin, E.: Convective rain cells: Radar-derived spatiotemporal characteristics and
577 synoptic patterns over the eastern Mediterranean, *J. Geophys. Res. D Atmos.*, 117,
578 10.1029/2011JD017353, 2012.

579 PETIT-MAIRE, N., BUROLLET, P. F., A BALLAIS, J.-L., A FONTUGNE, M., A ROSSO, J.-C., A LAZAAR, A.,
580 and Gauthier-Villars, I.: Paléoclimats holocènes du Sahara septentrional. Dépôts lacustres et
581 terrasses alluviales en bordure du Grand Erg Oriental à l'extrême-Sud de la Tunisie, *Comptes rendus*
582 *de l'Académie des sciences. Série 2, Mécanique, Physique, Chimie, Sciences de l'univers, Sciences de*
583 *la Terre* 312, 1661-1666, 1991.

584 Peyron, O., Jolly, D., Braconnot, P., Bonnefille, R., Guiot, J., Wirmann, D., and Chalieu, F.: Quantitative
585 reconstructions of annual rainfall in Africa 6000 years ago: Model-data comparison, *Journal of*
586 *Geophysical Research-Atmospheres*, 111, D24110
587 Artn d24110, 2006.

588 Prentice, I. C., and Jolly, D.: Mid-Holocene and glacial-maximum vegetation geography of the
589 northern continents and Africa, *Journal of Biogeography*, 27, 507-519, 2000.

590 Revel, M., Ducassou, E., Grousset, F. E., Bernasconi, S. M., Migeon, S., Revillon, S., Mascle, J., Murat,
591 A., Zaragosi, S., and Bosch, D.: 100,000 Years of African monsoon variability recorded in sediments of
592 the Nile margin, *Quaternary Science Reviews*, 29, 1342-1362, 10.1016/j.quascirev.2010.02.006,
593 2010.

594 Rogerson, M., Schönfeld, J., and Leng, M.: Qualitative and quantitative approaches in
595 palaeohydrography: A case study from core-top parameters in the Gulf of Cadiz, *Marine Geology*,
596 280, 150-167, 2011.

597 Rogerson, M., Rohling, E. J., Bigg, G. R., and Ramirez, J.: Palaeoceanography of the Atlantic-
598 Mediterranean Exchange: Overview and first quantitative assessment of climatic forcing. , *Reviews*
599 *of Geophysics*, 50, DOI: 8755-1209/8712/2011RG000376, 2012.

600 Rohling, E., Marino, G., and Grant, K.: Mediterranean climate and oceanography, and the periodic
601 development of anoxic events (sapropels), *Earth-Science Reviews*, 143, 62-97, 2015.

602 Rohling, E. J., and Bryden, H. L.: Estimating past changes in the Eastern Mediterranean freshwater
603 budget, using reconstructions of sea level and hydrography, *Proceedings Koninklijke Nederlandse*
604 *Akademie van Wetenschappen, Serie B*, 97, 201-217, 1994.

605 Rowan, J. S., Black, S., Macklin, M. G., Tabner, B. J., and Dore, J.: Quaternary environmental change
606 in Cyrenaica evidenced by U-Th, ESR and OSL of coastal alluvial fan sequences. , *Libyan Studies*, 31,
607 5-16, 2000.

608 Schwarcz, H. P., Harmon, R. S., Thompson, P., and Ford, D. C.: Stable isotope studies of fluid
609 inclusions in speleothems and their paleoclimatic significance, *Geochimica et Cosmochimica Acta*,
610 40, 657-665, [http://dx.doi.org/10.1016/0016-7037\(76\)90111-3](http://dx.doi.org/10.1016/0016-7037(76)90111-3), 1976.

611 Smith, J. R., Giegengack, R., Schwarcz, H. P., McDonald, M. M. A., Kleindienst, M. R., Hawkins, A. L.,
612 and Churcher, C. S.: A reconstruction of quaternary pluvial environments and human occupations
613 using stratigraphy and geochronology of fossil-spring tufas, Kharga Oasis, Egypt, *Geoarchaeology-an*
614 *International Journal*, 19, 407-439, 2004.

615 Smith, J. R., Hawkins, A. L., Asmerom, Y., Polyak, V., and Giegengack, R.: New age constraints on the
616 Middle Stone Age occupations of Kharga Oasis, Western Desert, Egypt, *Journal of Human Evolution*,
617 52, 690-701, 2007.

618 Swezey, C.: Eolian sediment responses to late Quaternary climate changes: temporal and spatial
619 patterns in the Sahara, *Palaeogeography, Palaeoclimatology, Palaeoecology*, 167, 119-155, 2001.

620 Toucanne, S., Angue Minto'o, C. M., Fontanier, C., Bassetti, M.-A., Jorry, S. J., and Jouet, G.: Tracking
621 rainfall in the northern Mediterranean borderlands during sapropel deposition, *Quaternary Science*
622 *Reviews*, 129, 178-195, <http://dx.doi.org/10.1016/j.quascirev.2015.10.016>, 2015.

623 Tuenter, E., Weber, S. L., Hilgen, F. J., and Lourens, L. J.: The response of the African summer
624 monsoon to remote and local forcing due to precession and obliquity, *Global and Planetary Change*,
625 36, 219-235, 2003.

626 Vaks, A., Woodhead, J., Bar-Matthews, M., Ayalon, A., Cliff, R., Zilberman, T., Matthews, A., and
627 Frumkin, A.: Pliocene–Pleistocene climate of the northern margin of Saharan–Arabian Desert
628 recorded in speleothems from the Negev Desert, Israel, *Earth and Planetary Science Letters*, 368, 88-
629 100, 2013.

630 Van Breukelen, M., Vonhof, H., Hellstrom, J., Wester, W., and Kroon, D.: Fossil dripwater in
631 stalagmites reveals Holocene temperature and rainfall variation in Amazonia, *Earth and Planetary
632 Science Letters*, 275, 54-60, 2008.

633 Wainer, K., Genty, D., Blamart, D., Daëron, M., Bar-Matthews, M., Vonhof, H., Dublyansky, Y., Pons-
634 Branchu, E., Thomas, L., van Calsteren, P., Quinif, Y., and Caillon, N.: Speleothem record of the last
635 180 ka in Villars cave (SW France): Investigation of a large $\delta^{18}\text{O}$ shift between MIS6 and MIS5,
636 *Quaternary Science Reviews*, 30, 130-146, <http://dx.doi.org/10.1016/j.quascirev.2010.07.004>, 2011.

637 Wassenburg, J. A., Immenhauser, A., Richter, D. K., Niedermayr, A., Riechelmann, S., Fietzke, J.,
638 Scholz, D., Jochum, K. P., Fohlmeister, J., Schröder-Ritzrau, A., Sabaoui, A., Riechelmann, D. F. C.,
639 Schneider, L., and Esper, J.: Moroccan speleothem and tree ring records suggest a variable positive
640 state of the North Atlantic Oscillation during the Medieval Warm Period, *Earth and Planetary Science
641 Letters*, 375, 291-302, <http://dx.doi.org/10.1016/j.epsl.2013.05.048>, 2013.

642 Wassenburg, J. A., Dietrich, S., Fietzke, J., Fohlmeister, J., Jochum, K. P., Scholz, D., Richter, D. K.,
643 Sabaoui, A., Spötl, C., Lohmann, G., Andreae, Meinrat O., and Immenhauser, A.: Reorganization of
644 the North Atlantic Oscillation during early Holocene deglaciation, *Nat. Geosci.*, 9, 602,
645 10.1038/ngeo2767

646 <https://www.nature.com/articles/ngeo2767#supplementary-information>, 2016.

647

648

649

650

651 Figure Captions

652 Figure 1: Map showing the location of Susah Cave (filled circle) and GNIP sites used in the discussion
653 (open circles). Blue stars indicate sources of marine water evaporation discussed in the text. Grey
654 arrows indicate recent average winter wind direction.

655 Figure 2) Macroscopic structure of SC-06-01 speleothem, showing alternation of transparent and
656 milky fabrics

657 Figure 3) Variability of water content (μL) per unit mass of speleothem (g) in SC-06-01 fluid inclusion
658 samples. Grey area shows working range of instrument.

659 Figure 4a) Fluid inclusion oxygen isotope values ($\delta^{18}\text{O}_{\text{fi}}$; black crosses) compared to calcite oxygen
660 isotope values ($\delta^{18}\text{O}_{\text{cc}}$; blue circles and line); 4b) Fluid inclusion hydrogen isotope values ($\delta^2\text{H}_{\text{fi}}$; black
661 crosses) compared to $\delta^{18}\text{O}_{\text{cc}}$ (blue circles and line). Growth Phases I, II and III are shown as grey
662 areas.

663 Figure 5a) Regional precipitation isotope data. Thick line represents Global Meteoric Water Line,
664 dashed thick line represents Mediterranean Meteoric Water Line and thin lines representing
665 expected range of deviation ($\pm 10\text{‰ } \delta^2\text{H}_{\text{ppt}}$) below GMWL and above MMWL. Bet Dagan, Tunis and
666 Sfax GNIP datasets (http://www-naweb.iaea.org/napc/ih/IHS_resources_gnip.html). Sfax Atlantic

667 and Mediterranean Rainfall are taken from Celle-Jeanton et al. (2001). 5b-d) Summarised
668 precipitation isotopes, and fluid inclusion measurements for SC-06-01 for Phases I, II and II
669 respectively.

670 Figure 6) Double-replicated fluid inclusion measurements from SC-06-01, and regional precipitation
671 isotope trends.

672 Figure 7) $^{87}\text{Sr}/^{86}\text{Sr}$ record for SC-06-01, compared to calcite $\delta^{18}\text{O}_{\text{cc}}$ record (light grey line). Error bars
673 are 2σ . Growth Phases I, II and III are shown as grey areas.

674 Figure 8) Carbon isotope ($\delta^{13}\text{C}_{\text{cc}}$) record for SC-06-01 compared to oxygen isotope record ($\delta^{18}\text{O}_{\text{cc}}$;
675 (Hoffmann et al., 2016)). Growth Phases I, II and III are shown as grey areas.

676 Figure 9) Fluid inclusion measurements relative to summarised precipitation data and the modern
677 precipitation end members used in the discussion. Solid lines are the Meteoric Water Lines as in Fig.
678 5a. Precipitation and fluid inclusion measurements are as shown in Figure 5b. "Mean Atlantic", "Sfax
679 Mixed", "Sfax Med" and "High Precip Atlantic" indicate the mean of measurements in Celle-Jeanton
680 et al. (2001) originating from Atlantic moisture, mixed source, Mediterranean moisture and High
681 Precipitation measurements from an Atlantic moisture source (as described in Discussion)
682 respectively. "Mean Bet Dagan" is the mean of GNIP measurements from this location, and "High
683 Precip Bet Dagan" is the subset of high precipitation measurements as described in the Discussion.

684 Figure 10) Fluid inclusion deuterium excess ($\delta^2\text{H}_{\text{excess-Fi}}$) relative to calcite $\delta^{18}\text{O}_{\text{cc}}$. Note some fluid
685 inclusions (70 to 60 ka BP and 40 to 30 ka BP) show high ($\delta^2\text{H}_{\text{excess-Fi}}$) indicative of an Eastern
686 Mediterranean source. Growth Phases I, II and III are shown as grey areas.

687

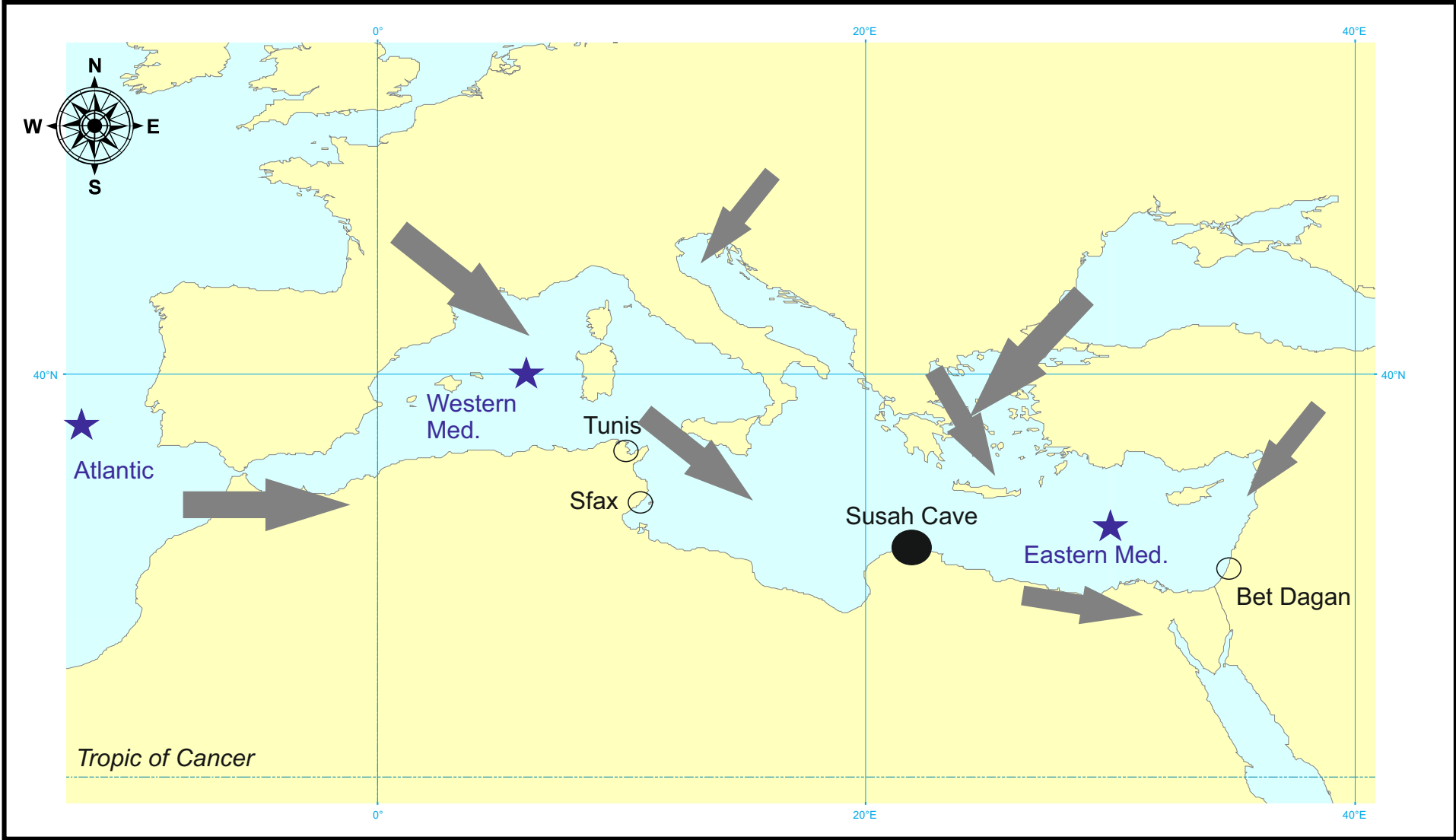


Figure 2

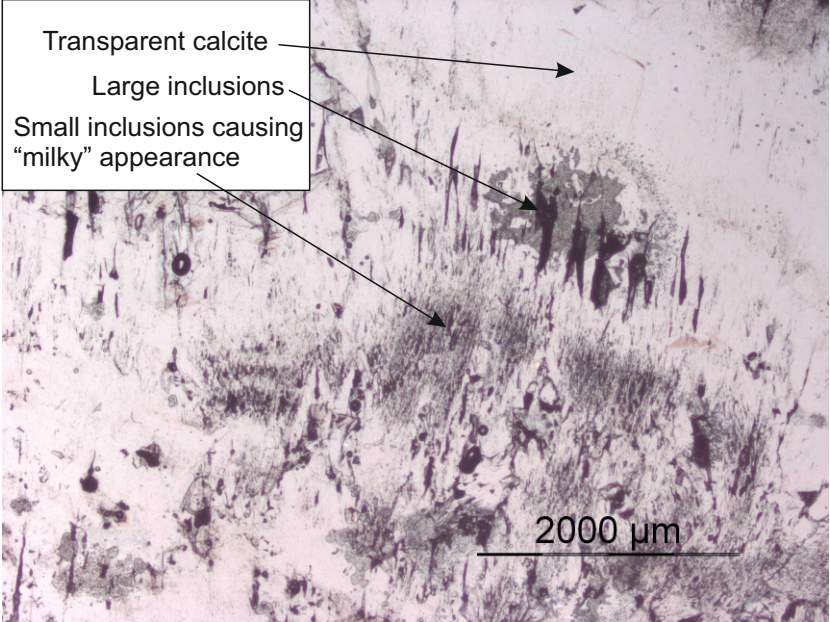


Figure 3

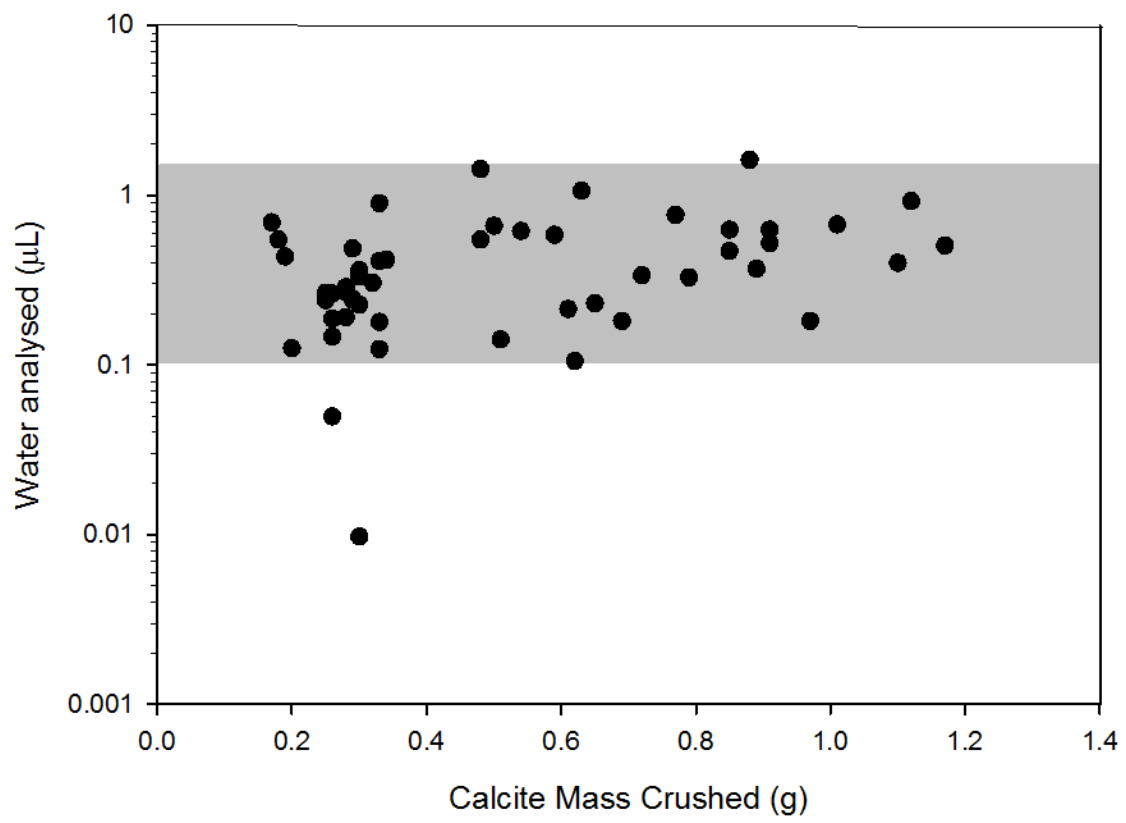


Figure 4a

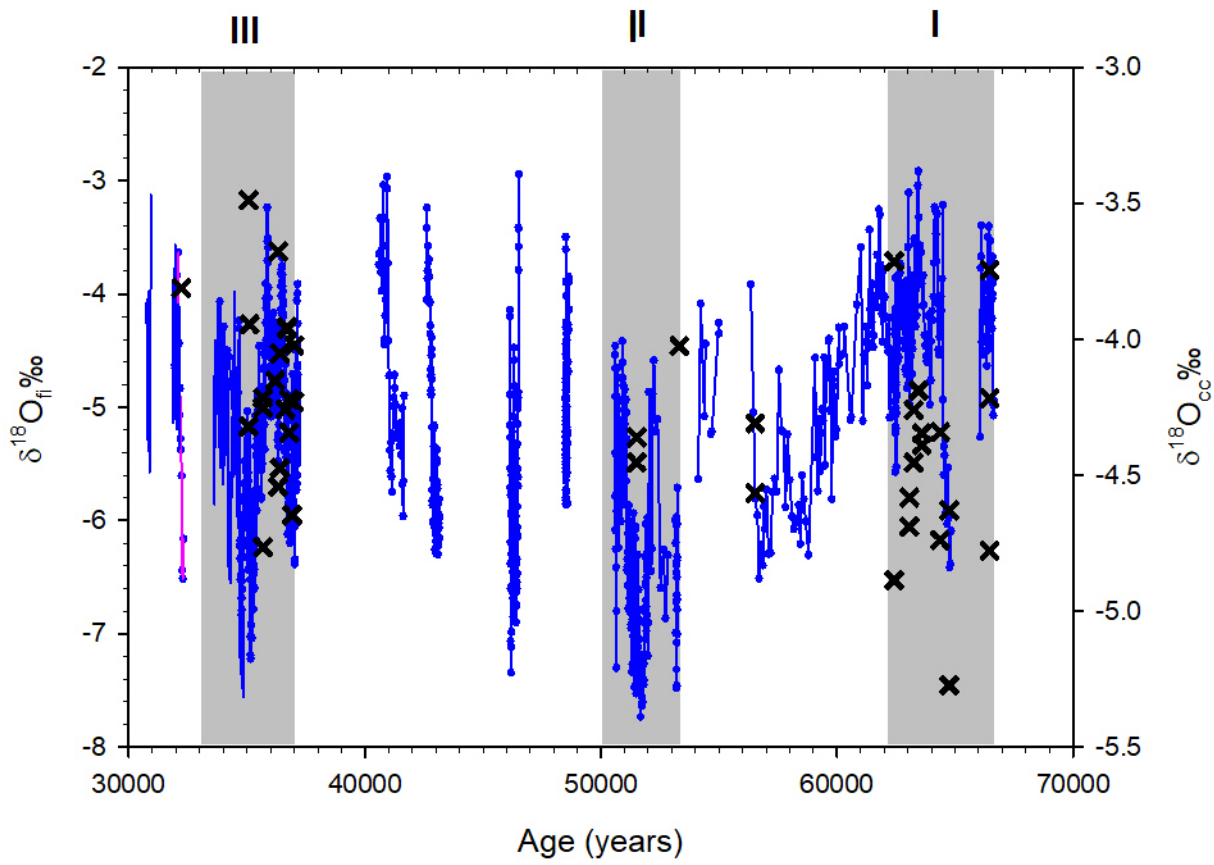


Figure 4b

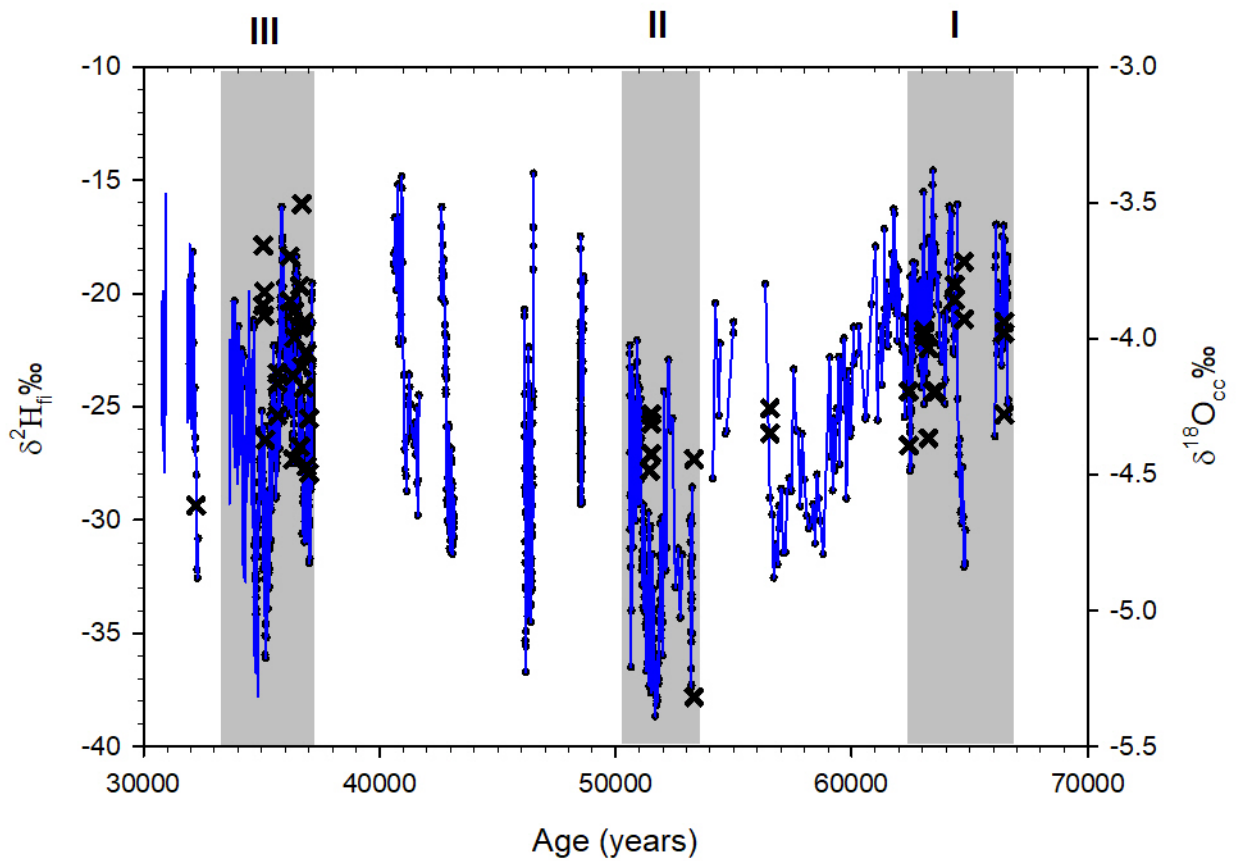


Figure 5a

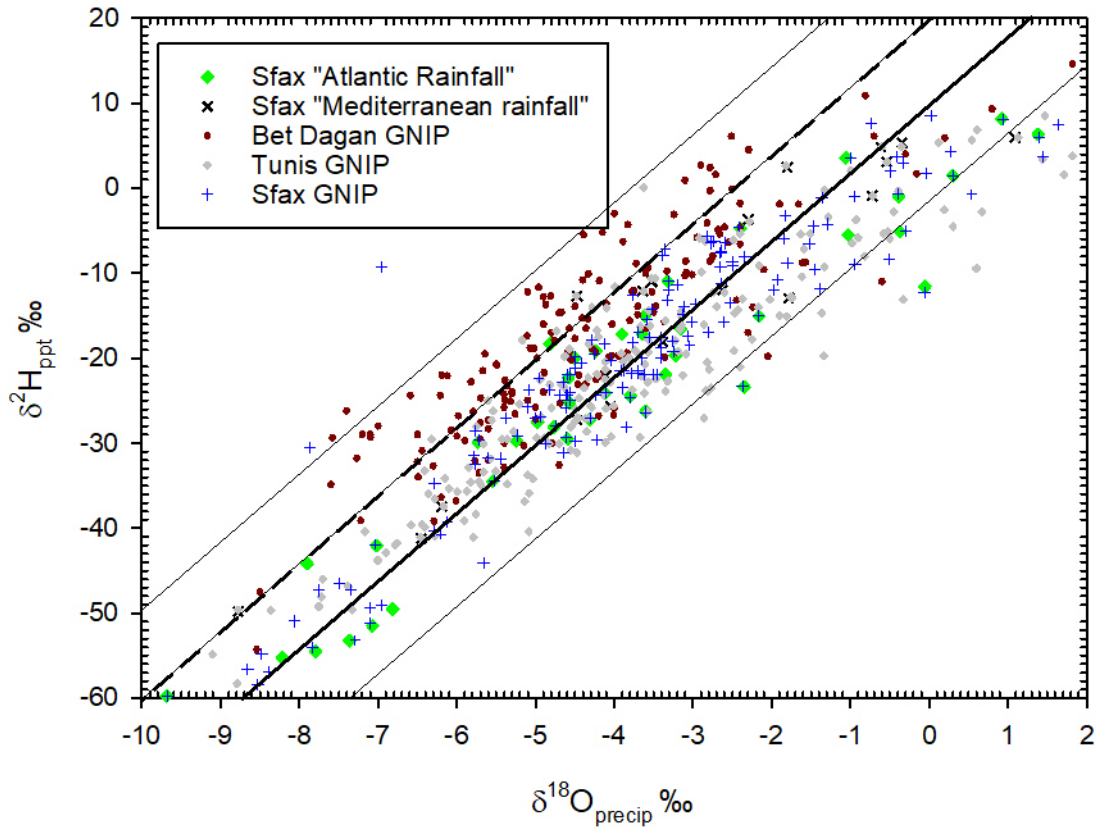


Figure 5b

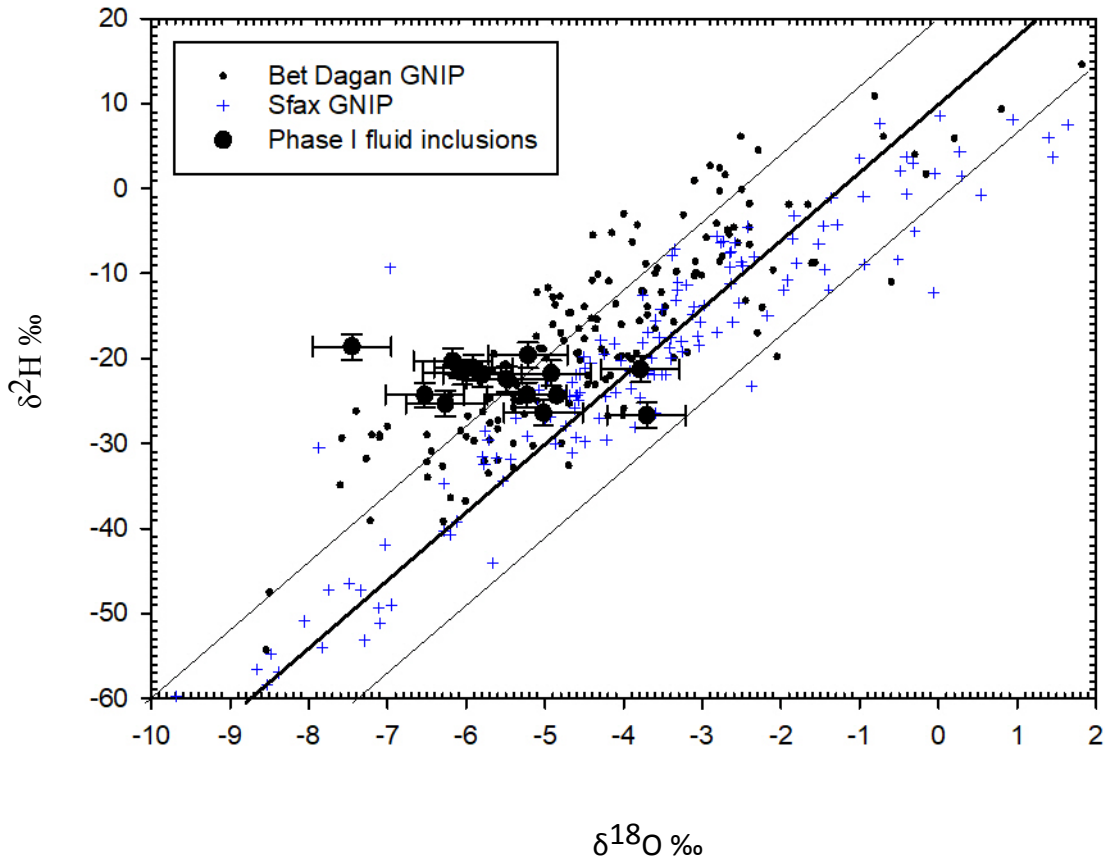


Figure 5c

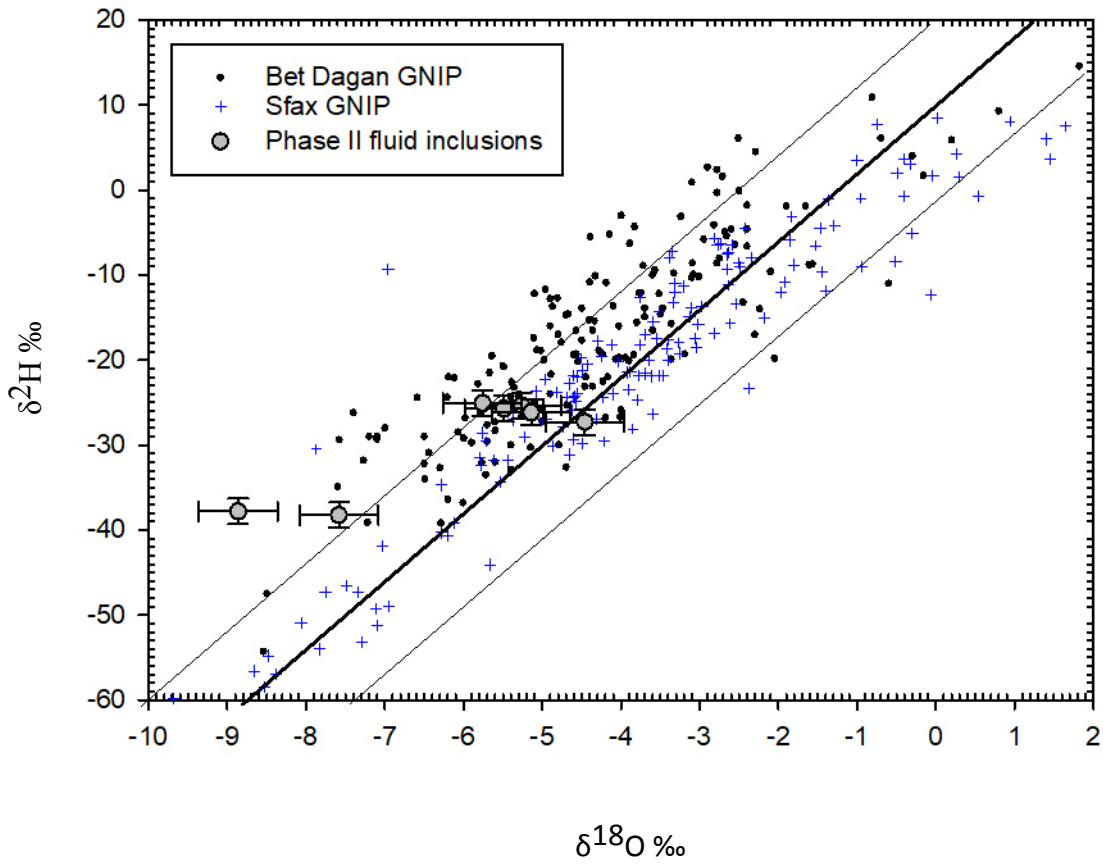


Figure 5d

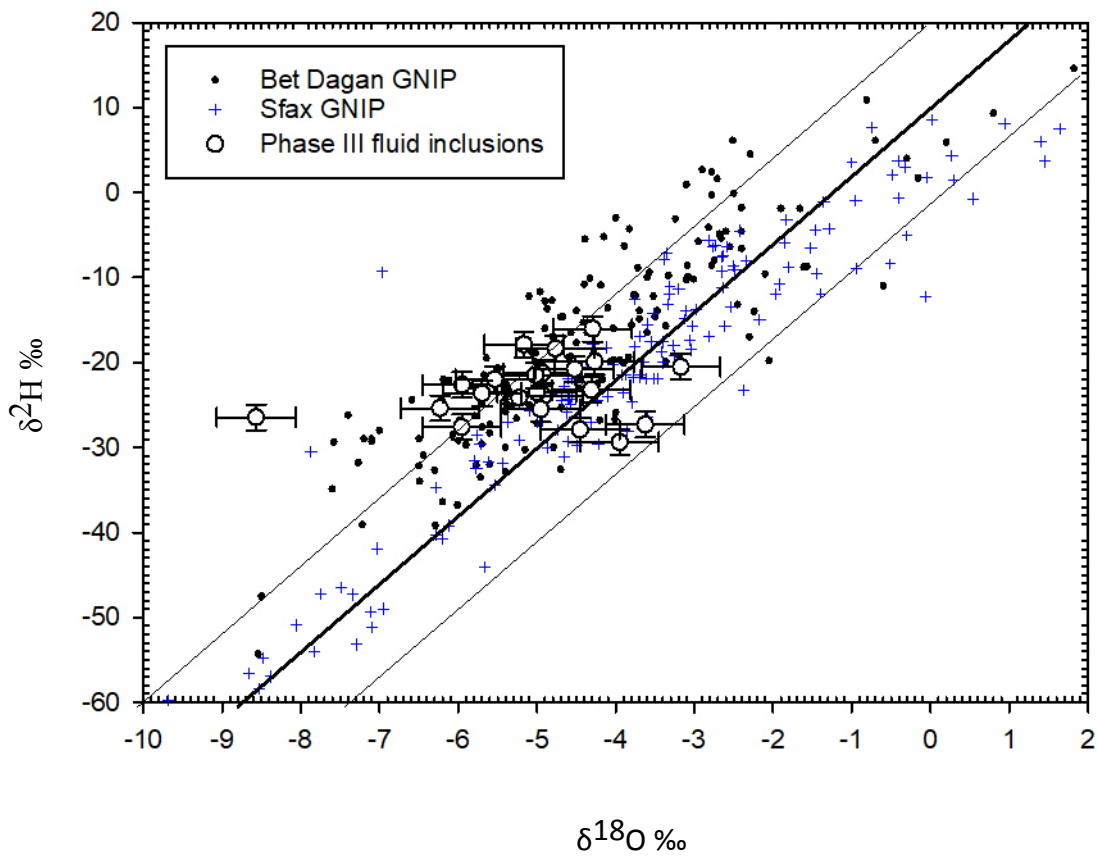


Figure 6

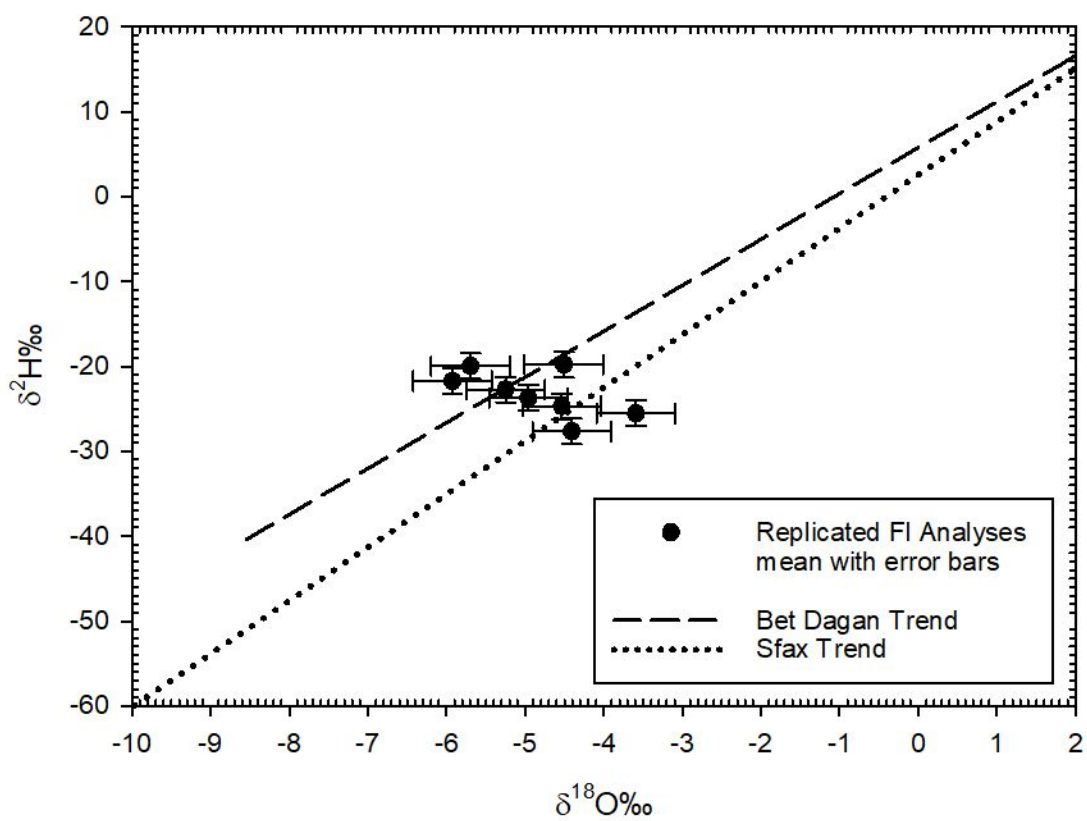
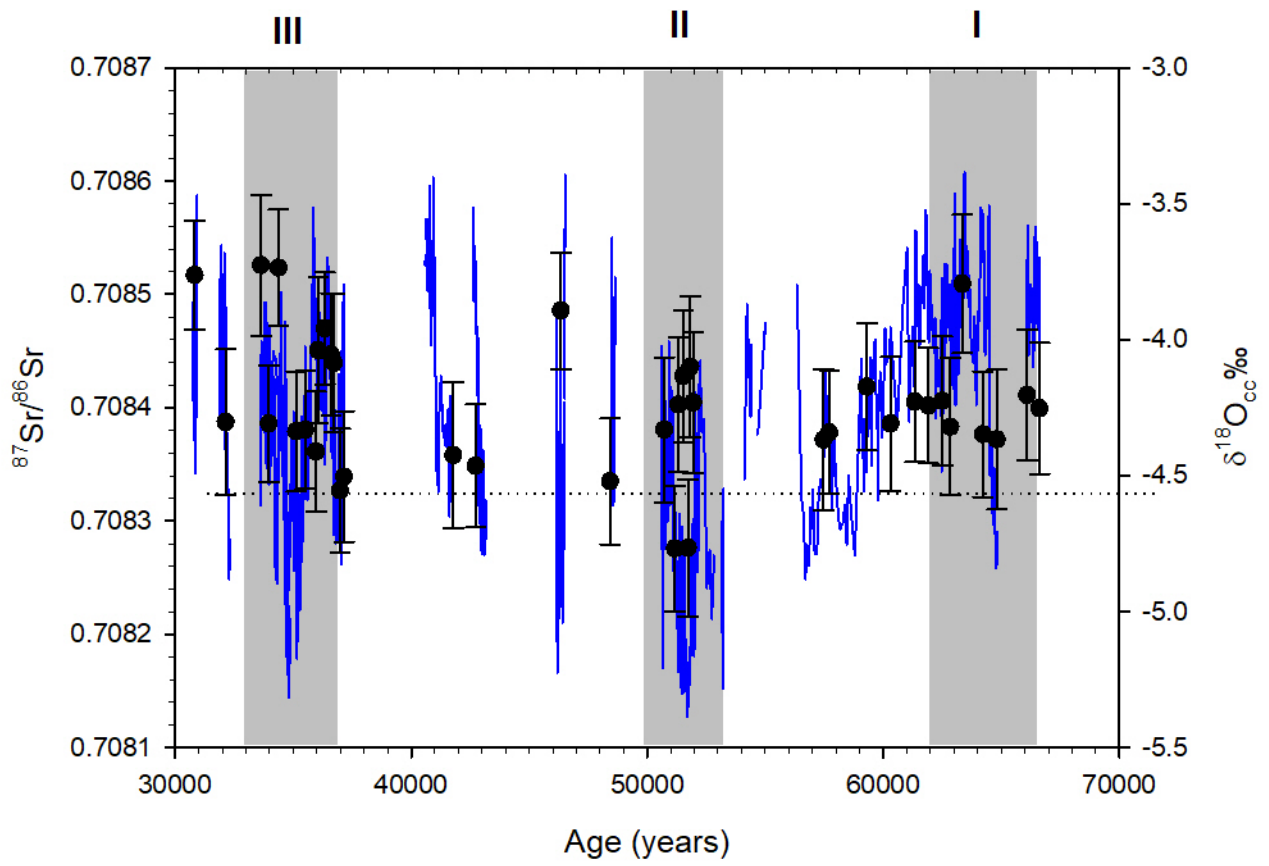


Figure 7



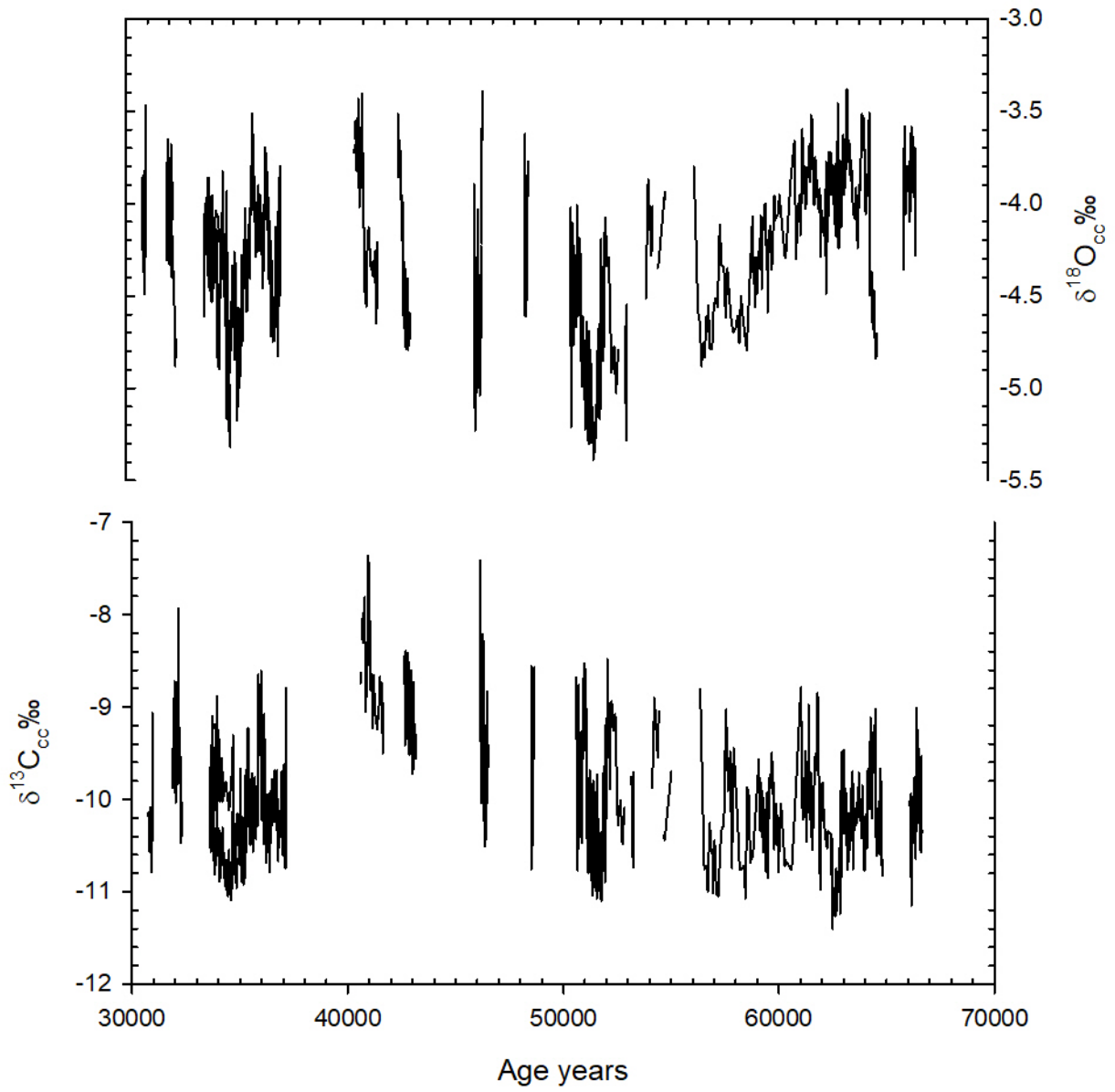


Figure 9

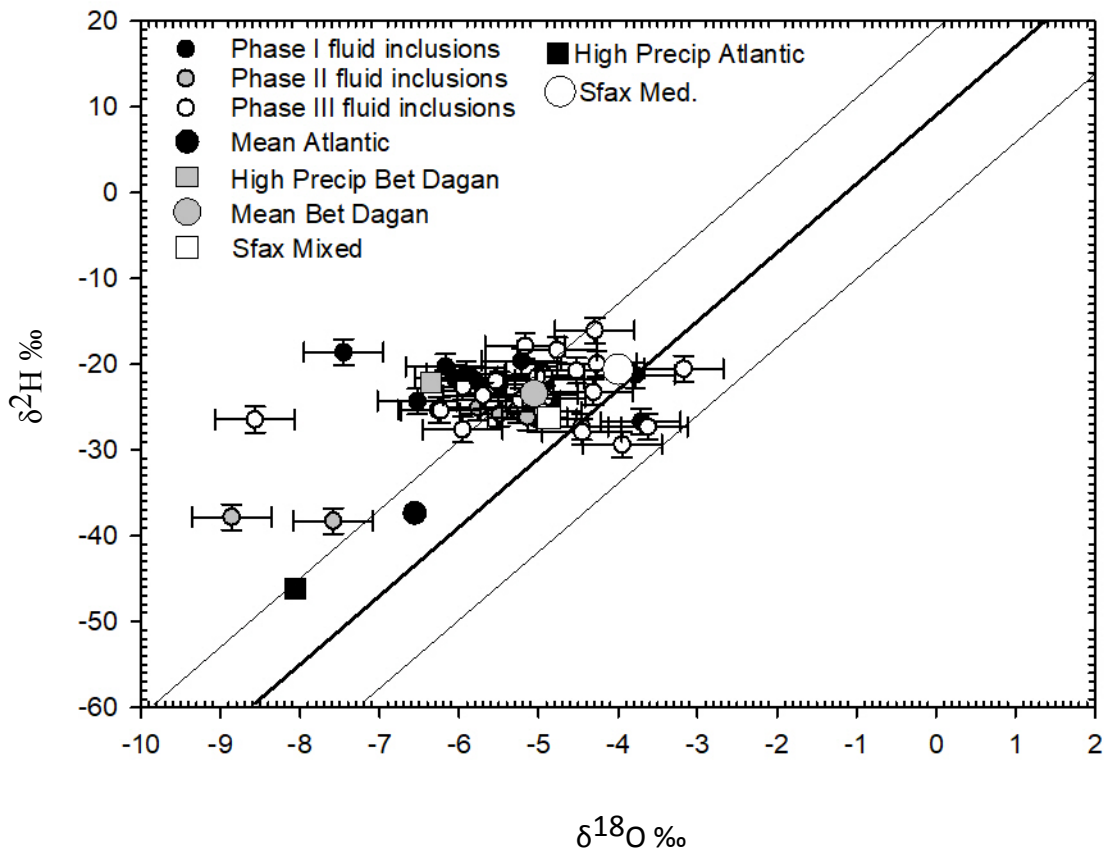


Figure 10

